Fifth International Symposium on Marine Propulsion
smp'17, Espoo, Finland, June 2017

VOF Simulations Of Hydrodynamic Cavitation Using The Asymptotic And Classical Rayleigh-Plesset Models

Samir Muzaferija[1], Dimitrios Papoulias[2], Milovan Peric[1]

[1]Siemens Industry Software GmbH, Nordostpark 3-5, Nuremberg 90411, Germany
[2]Siemens PLM Software, 200 Shepherds Bush Road, London W6 7NL, UK

ABSTRACT

In this paper a computational analysis of the dynamic vortex-cavitation flow observed on the so-called twist-11 Delft hydrofoil (Foeth 2008) is presented. Flow calculations are performed using Reynolds-Averaged Navier-Stokes (RANS) as well as Improved Delayed Detached-Eddy simulation (IDDES) models available in the commercial software STAR-CCM+. The flow-field is realized as a continuous mixture of liquid and vapor bubbles, in the context of the Eulerian Volume of Fluid (VOF) method. For predicting growth/collapse oscillations of cavitation bubbles, the multiphase VOF solver is coupled with different cavitation models based on the Rayleigh-Plesset (R-P) equation. Parametric simulations tested include the asymptotic formulation proposed by Sauer (2000) and the classical R-P equation, which also accounts for the inertia of bubbles as well as surface-tension and viscous effects (Brennen 1995). The obtained results are validated against reported experimental measurements in terms of the lift force and the vortex shedding frequency. In addition, model predictions are also compared against equivalent Computational Fluid Dynamic (CFD) simulations reported in the literature (Hoekstra et al 2011, Bensow 2011). The evaluation of the predicted results suggests that inertial effects of cavitating bubbles have a major impact on the transient characteristics of multiscale vortex cavitation flows.

Keywords

DES, Vortex-cavitation, Rayleigh-Plesset model

1 INTRODUCTION

The development of dynamic cavitation structures in marine propulsors and hydrodynamic control surfaces is linked to undesirable effects, responsible for loss of thrust, noise and vibrations as well as material damage due to erosion. To a certain extent, experimental techniques and CFD models provide useful results for understanding the physics governing hydrodynamic cavitation in turbulent flows.

An insightful analysis of experiments in vortex cavitation flows is documented in the work reported by Arndt (1995). The examined research in this manuscript is mainly focused on the derivation of cavitation scaling-laws as well as the observation of cavitation structures, manifesting at the tip and trailing vortices of propellers and hydrofoils. Presented results for different Reynolds (Re) and cavitation (σ) numbers indicate that the inception and development of vortical cavitation exhibits a complex dependency on the water quality, the induced turbulent fluctuations in the vortex region as well as the surface-tension of preexisting nuclei (Arndt & Keller 1992). In the majority of the cases, the developed theoretical laws rely on idealized vortex flow models (Bachelor 1967, Lamb 1979), thus prohibiting the realization of the inception process and the interaction dynamics of bubbles in vortices (Arndt et al 1991, Boulon et al 1999).

Despite the complex physics, the dedicated research in two-phase vortex flows has facilitated the identification of the main cavitation types and shedding mechanisms (Knapp, Daily & Hammit 1970). At high incidence angles and Reynolds numbers, cavitation in hydrofoil flows appears at the leading edge in the form of an unsteady partial cavity. In some cases a re-entrance jet locally impinges on the interface of the cavity, causing periodic shedding of bubble clouds which collapse at the wake (Laberteaux & Ceccio 2001). With the aid of high-speed visualizations and Laser Doppler velocimetry (LDV), Avellan and Dupond (1991) deduced that the intermittent shedding of discrete bubble formations originates from the interference between the cavity trailing edge and spanwise vortex filaments generated at the wall. Due to growing surface instabilities (Kelvin-Helmholtz) and energy inputs from the mean-flow, the swirling bubbly structures stretch and evolve into horseshoe-type vapor vortices with their core U-shaped body oriented at an angle towards the effective flow (Head & Bandyopadhyay 1980). Similar vortex cavitation structures are also observed in the water tunnel experiments performed by Foeth and Terwisga (2006), using a twisted NACA hydrofoil. The results collected from this study confirmed that the breakup of the partial cavity is mainly triggered by the development of a re-entrance jet, which is directed against the closure region of the cavitation sheet driven by a strong adverse pressure gradient. According to Callenaere et al (2001), the strong pressure wave developing at the concave closure boundary of the cavity is a physical necessity and together with the

thickness size of the forming vapor sheet controls the onset of re-entrance jet instabilities.

A new mechanism for sheet-to-cloud transition of partial cavities in wedge-obstacle cavitation flows is suggested in the experiments conducted by Ganesh et al (2016). By using X-ray densitometry and placing pressure probes below the cavitation sheet, the authors of this work deduced that for high vapor volume-fractions the speed of sound within the bubbly mixture dropped significantly, promoting in this way strong shock-waves from the collapsing cavities. The shock-wave front propagated upstream and eventually impinged against the cavitation inception corner, causing the sheet cavity to disintegrate into a large cluster of bubbles.

For modelling cavitation effects in fluids two basic Eulerian homogeneous methodologies are favored in the research community. The most general is based on the classical Rayleigh-Plesset equation (R-P) for the prediction of cavitation growth/collapse bubble-dynamics (Rayleigh 1919, Plesset 1949). Typical VOF and mixture multiphase flow solvers are coupled with the asymptotic R-P model, thereby neglecting the inertial term as well as effects due to surface-tension and viscous diffusion. Such models are proposed by Sauer (2000), Singhal et al (2002) and Zwart et al (2004); the main difference being that each one is tailored with individual correction terms, which accounted for tension effects due to turbulent pressure fluctuations and damping arising from the presence of non-condensable gas. Coutier-Delgosha et al (2003a) and Schmidt (2009) pursued a different approach for modelling phase-change effects in cavitating flows, based on thermodynamic equilibrium principles. In this context, the genesis and collapse of cavitation bubbles is effectively modeled as an evaporation/condensation mass-transfer process with the aid of a barotropic equation of state. Simulation results reported in the literature using the aforementioned models (Ji et al 2013, Gnanaskandan 2016, Schnerr et al 2008, Coutier-Delgosha 2003b) appear to be consistent with corresponding experiments in vortex cavitation flows.

Part of the success of Eulerian two-phase models in cavitation flows is attributed to the solution techniques used for resolving turbulence, which mostly involved large-eddy (LES) and detached-eddy (DES) simulations. Multiphase RANS methods based on typical two-equation turbulence models, were less fortunate in mimicking the transient characteristics of vortex cavitation flows. Reboud et al (1998) argued that the no-slip condition assumed between the flow-phases is responsible for the artificial stabilization of the cavitation shedding. To compensate for this modelling limitation, the authors proposed an empirical eddy-viscosity modification, which effectively reduced the turbulence dissipation in the cavitation sites as a function of the vapor volume-fraction. Despite the fact that this correction recovered the unsteady behavior of the cavitating vortex flow, Bensow (2011) showed that the eddy-viscosity levels predicted with the aforementioned treatment contradict the respective levels calculated with DES as well as RANS models.

In the current study similar CFD methods are pursued for calculating the dynamic cavitation flow developing over the twisted Delft hydrofoil. The utilized multiphase models and turbulence closures are discussed in the next section.

2 MULTIPHASE VOF MODEL

In the context of the Eulerian VOF approach, multiphase flows are realized as homogeneous mixtures consisting of immiscible fluid phases. Based on this assumption, the continuous and dispersed phases can be effectively lumped into a single continuum, sharing the same pressure and velocity fields. For incompressible mixtures the governing equations for the continuity and momentum are formulated in the following form:

$$\frac{\partial \rho_m}{\partial t} + \nabla(\rho_m \mathbf{u}) = 0 \tag{1}$$

and

$$\frac{\partial}{\partial t}(\rho_m \mathbf{u}) + \nabla\cdot(\rho_m \mathbf{u}\otimes\mathbf{u} - \mathbf{T}) = \rho_m \mathbf{g} + \mathbf{f}_s \tag{2}$$

where t is the time, **u** is the velocity vector of the mixture, **T** is the stress tensor including the pressure term, **g** is the gravitational acceleration and $\mathbf{f}_s$ stands for the surface-tension force. The mixture density ρ_m and viscosity μ_m are volume-averaged in terms of the local volume-fraction α:

$$\phi_m = \sum_i \alpha_i \phi_i \tag{3}$$

where ϕ_m denotes a generic thermodynamic property of the mixture (e.g. density, etc.) and the subscript *i* denotes the different phases. The fields of phase volume fractions α_i feature in the phase mass conservation equation:

$$\frac{\partial}{\partial t}(\rho_i \alpha_i) + \nabla\cdot\rho_i(\alpha_i \mathbf{u}) = \mathbf{S}_{\alpha_i} \tag{4}$$

where $\mathbf{S}_{\alpha_i}$ is a source/sink term for the phase *i*. The volume fraction of the different phases *i* varies from 0 to 1 in the field and, by definition, the summation at each cell *c* must be equal to 1:

$$\sum_i^c \alpha_i = 1 \tag{5}$$

Equations (1-5) are discretized and solved in a segregated manner using the finite-volume technique.

2.1 Cavitation Models

The production rate of cavitation vapor, which appears as a mass source-term in the volume-fraction conservation equation (Equation 4: $\mathbf{S}_{\alpha_i}$), is approximated with the R-P model following a seed-based mass transfer approach. In this modelling technique, the liquid phase is assumed to be contaminated with populations of nuclei seeds, which constitute the precursors of cavitation bubbles. The pre-existing bubble embryos are presumed to be spherical in shape and with the same initial size (R_0), coexisting with the surrounding flow at equilibrium conditions. Bubble growth is triggered at locations where the flow is subjected to tension, which exceeds the effective tensile strength of

the liquid phase. In practical experiments and applications, the incipience of cavitation bubbles occurs at weak points in the fluid continuum (e.g. impurities and dissolved gas), when the fluid pressure drops to saturation vapor levels (p_v). Once this physical limit is reached, cavitation vapor is produced or consumed at a rate proportional to the growth/collapse oscillations of the newborn cavitation bubbles. Accordingly, the generation of cavitation vapor in discrete volume cells V_c under-tension ($p<p_v$) is defined as:

$$\mathbf{S}_{\alpha_i} = N\frac{\mathrm{dV_b}}{\mathrm{dt}}\rho_i = 4\pi n_0 \rho_i \alpha_l V_c \mathrm{R}^2 \frac{\mathrm{DR}}{\mathrm{Dt}} \qquad (6)$$

where N is the number of bubble seeds, n_0 is the bubble number-density, V_b is the volume of a single bubble, index l denotes the liquid phase and R is the bubble radius. The growth/collapse size of spherical cavitation bubbles can be estimated simply by considering the cell volume occupied by the vapor phase (α_g):

$$\mathrm{R} = \left(\frac{\alpha_g}{4/3\,\pi n_0 \alpha_l}\right)^{1/3} \qquad (7)$$

The remaining time-derivative term in Equation (6) stands for the bubble radial velocity (u_r). This unknown parameter is calculated by solving the R-P equation:

$$\mathrm{R}\frac{\mathrm{du_r}}{\mathrm{dt}} + \frac{3}{2}\mathrm{u_r^2} = \frac{\mathrm{p_v} - \mathrm{p_\infty}}{\rho_l} - \frac{2\sigma}{\rho_l \mathrm{R}} - 4\frac{\mu_l}{\rho_l \mathrm{R}}\mathrm{u_r} \qquad (8)$$

where p_∞ is the pressure of the undistributed flow, σ the surface-tension coefficient and μ the dynamic viscosity. By expanding the material derivative of the inertial term, Equation (8) can be rearranged into a quadratic form for the variable u_r and solved iteratively using an implicit Euler scheme.

A less rigorous cavitation model for the solution of the bubble growth/collapse velocity is the asymptotic R-P equation, adopted in the Schnerr-Sauer model (S-S). In this approach the classical R-P equation is effectively reduced to an algebraic expression by neglecting the non-linear inertial term as well as bubble-dynamic effects attributed to viscosity and surface-tension:

$$\mathrm{u_r} = \mathbf{sign}(\mathrm{p_v} - \mathrm{p_\infty})\left(\frac{2}{3}\frac{|\mathrm{p_v} - \mathrm{p_\infty}|}{\rho_l}\right)^{1/2} \qquad (9)$$

The S-S R-P model formulated in Equation (9), provides the growth/collapse radial velocity as a function of the square-root of the pressure drop across the bubble surface. In the case of bubble growth, this equation represents the asymptotic solution of the R-P equation. However, when the surrounding pressure is larger than vapor pressure, the resulting collapse rate is not very realistic. In addition, discarding the inertial term can lead to overestimation of the oscillation bubble sizes, given the rapid rates at which bubbles grow and collapse in cavitation episodes.

2.2 Turbulence Model

The cavitation VOF model requires additional closures for the stress-term (**T**) in Equation 2. To this purpose, two different strategies are used: the two-equation Shear-Stress Transport model (SST) and the Improved Delayed Detached-Eddy Simulation approach (IDDES). In the first method turbulence is modelled via the Reynold-stresses, which are assumed isotropic and accordingly treated with the hybrid SST model proposed by Menter (1994). This method blends the revised k-ω model near the wall (Wilcox 2008) with the traditional k-ε formulation in the outer free-stream region and therefore inherits the advantages of both techniques. In addition, the SST model employs a modified eddy-viscosity model (Johnson & King 1985), which involves the solution of an ordinary differential equation for the transport of the principal turbulent stress.

The IDDES model combines features of the SST RANS technique with spatial filtering methods for the solution of the Navier-Stokes equations, including the Delayed-DES (DDES) and Wall-Modelled LES models (WMLES). In this hybrid RANS-LES approach, modelling of subgrid scale (SGS) turbulence and blending between the LES models is controlled by a hybrid expression for the eddy length-scale $l_{hyb.}$ as well as the new mesh filter Δ proposed by Shur et al (2008):

$$l_{hyb.} = \tilde{f}_d(1 + f_e)l_{RANS} + \left(1 - \tilde{f}_d\right)l_{LES} \qquad (10)$$

and

$$\Delta = min\{max[0.15d_w, 0.15h_{max}, h_{min}], h_{max}\} \qquad (11)$$

where f_e is the elevating function and $\tilde{f}_d$ is the blending function for the DDES and WMLES branches of the model. The former function addresses the mismatch between the resolved and modelled log-layer by adjusting the RANS component (l_{RANS}) of the hybrid length-scale. The LES length-scale is defined by the utilized filter and an empirical DES constant, $l_{LES} = C_{DES}\Delta$. To limit RANS modelling to a much thinner near-wall region, in addition to the blending function, the filter is also altered to accommodate the grid wall-distance (d_w). The remaining terms in Equation (11) stand for the local maximum grid spacing (h_{max}) and the minimum distance between neighboring cells (h_{min}).

3 SIMULATION FLOW-MODEL SETUP

Details regarding the twist-11 Delft foil geometry and the experimental flows simulated in the smp'11 workshop are available by Hoekstra et al (2011). The parametric RANS and IDDES cavitation simulations presented in this study are summarized in Table 1. The computational domain of the basic flow section is show in Figure 1.

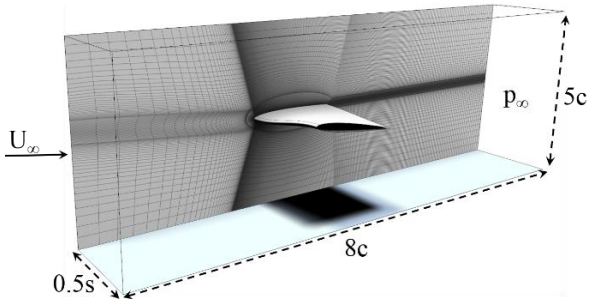

Figure 1: Discretized flow solution domain

In the considered flow scenario, water at room temperature (24 ^{o}C) is circulated inside the test-section of the tunnel at a speed of 6.97 m/s (U_∞) and a downstream pressure of 29 kPa (p_∞). The tested hydrofoil is a replica model derived from a symmetric NACA 0004, with 0.15 m chord (c) and a span of 0.3 m (s). To suppress cavitation near the tunnel wall, the wing is twisted along the span to shape a platform with a variable angle-of-attack. The rectangular wing is positioned at an angle inside the water tunnel test-section, resulting to a maximum 9^{o} rotation at the middle and -2^{o} at the mounted wall. The corresponding Re and σ numbers for this experiment are estimated to be 1.05E+06 and 1.07, respectively.

Table 1: Flow conditions and solution inputs

Turbulence model	Cavitation model	Solver inputs	Flow Conditions
SST k-ω	S-S & classical R-P	2nd order upwind 2nd order backward dt=1.0 μs	U_∞=6.97 m/s p_∞=29 kPa n_0=1.E12 (/m^3) R_0=1.0 μm
IDDES			

To ensure fully-developed flow conditions, the velocity inlet boundary is placed at distance 3c upstream of the wing's leading-edge. Likewise, the pressure-outlet plane is located 4c away from the trailing-edge, allowing sufficient downstream space for the wake to dissipate. In the present calculations only half the model is simulated, taking advantage of the symmetry of the problem. The solution domain is discretized with an O-H type grid, consisting of nearly 22 million cells. Particularly at the cavitating suction side, the grid near the hydrofoil is refined with successive layers of cells resulting to y^+ values in the range of 0.1 to 5.0. The water and cavitation vapor phases are modeled as incompressible materials, with their thermodynamic properties (ρ_i, μ_i) defined at the reference experimental temperature. Cavitation model inputs for the number-density (n_0) and nuclei-size (R_0) of the cavitation seeds are set according to approximations available in the literature, for the spectral bubble distributions found in typical liquids (Brennen 1995).

The governing equations are discretized using 2nd order accurate schemes in space and time, including the fully-implicit three-time-level technique for the unsteady terms and linear extrapolation method for the convective fluxes. For both RANS and IDDES simulations, a time-step of 1.0 μs was used. For the IDDES calculations, the initial flow-field is provided from single-phase predictions obtained with the k-ω SST model. A statistically steady-state is reached by averaging the solution for a sufficient number of cavitation shedding cycles. For predicting the growth/collapse dynamics of vapor bubbles two cavitation models are evaluated, the asymptotic S-S formulation as well as the classical R-P model.

4 CAVITATION FLOW RESULTS

Model predictions of the periodic vortex cavitation flow developing along the twist-11 hydrofoil are illustrated in Figure 2, for different solution time-steps. The plotted flow contours in this figure correspond to the instantaneous and mean pressure-field developing at the wing surface as well as the mid-section of the domain. The boundary of the calculated cavitation structures is indicated with a gray colored iso-surface, defined by a constant vapor volume-fraction equal to 0.1. As it can be seen in these simulation scenes, the hydrodynamic two-phase flow evolves into different types of cavitation structures in a transient manner.

During the inception phase, the hydrofoil is partly covered by a cavitation sheet formed by accumulating populations of growing bubbles, which originate from the tension site developing at the leading-edge. Gradually, the vapor sheet canopy extends downstream to obtain its fully-developed elliptical shape, reaching up to the mid-span position where it attaches to form a closure region characterized by a stagnation pressure front (Kawanami et al 1997). This flow feature resembles the high pressure area (red), predicted spanwise across the triple boundary between the wall, the water and the vapor phases (Figure 2a-2b). The pressure gradient and turbulent eddies acting along this attachment boundary cause the flow to locally reverse, and detach into separated re-entrance jets which entrain the vapor cavity starting from the lateral sides (Foeth & Terwisga 2006). The resolution of the cavitation flow dynamics following the onset of the radial re-entrance jets, is found to be dependent on the physical assumptions of the utilized CFD models.

In agreement to previous studies (Bensow 2011), the S-S cavitation model and typical two-equation RANS closures appear to be insufficient to predict the transition from sheet cavitation to unsteady vortical shedding of detached bubbly clouds. Instead, this modelling approach predicted a continuous cavitation sheet, which performed weak growth/collapse oscillations (Figure 2d). However, the aforementioned asymptotic cavitation model seems to capture the dynamic shedding of bubble clusters when combined with the IDDES method (Figure 2b). Similar findings in the literature regarding the S-S cavitation model (Reboud et al 1998), lead to the impression that the limitation in mimicking the unsteady nature of this kind of flows is a deficit of the turbulence closure strategies used in RANS models. Despite the fact that this hypothesis is mostly true, the RANS results obtained with the classical R-P cavitation model appear to capture the transient shedding mechanism (Figure 2c). This suggests that the inertial term, which is omitted in the S-S formulation, is also responsible for inducing cyclic bubble perturbations strong enough to trigger the fragmentation and shedding of the vapor sheet.

Realization of the multiscale cavitation structures manifesting after the break-up of the vapor sheet, including the repeatable collapse episodes of bubbles as well as the discrete interactions of turbulent vortices with shedding bubble clouds, requires access to the instantaneous information of the flow. To a certain extent, details regarding these cavitation flow mechanisms are exposed in

the IDDES calculations. Collapsing cavitation clouds are detected in locations dominated by sudden pressure spikes, appearing across the disintegrating vapor sheet as well as the wake (Figure 2a-2b). Vortex-bubble interactions are illustrated in Figure 3, in terms of the calculated vorticity flow-field and cavitation clouds.

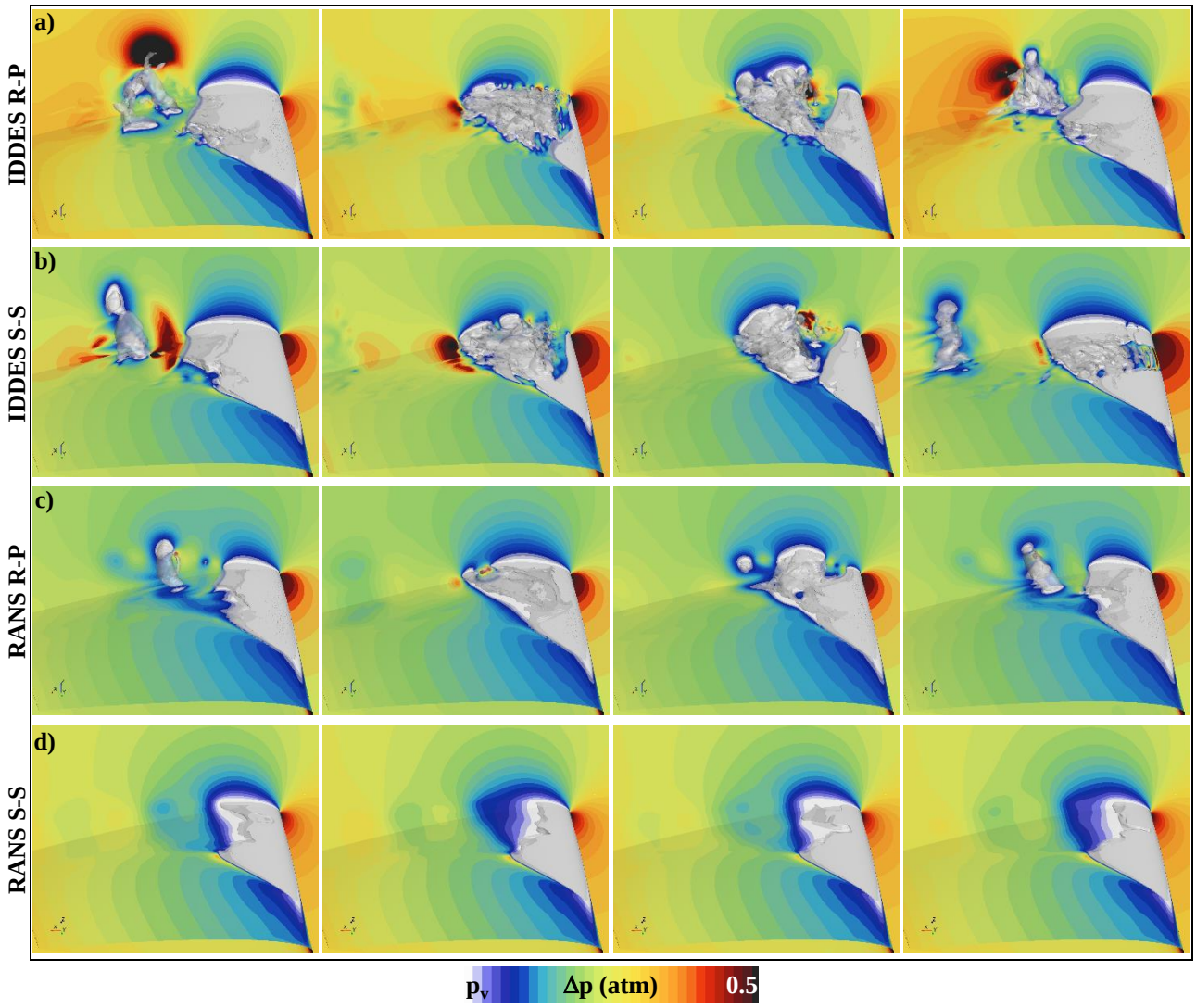

Figure 2: IDDES and RANS calculations using the R-P and S-S cavitation models; pressure contours and cavitation vapor

The volume-rendering plot in Figure 3 displays the instantaneous vorticity field of the cavitating hydrofoil, obtained with the IDDES approach and the suggested classical R-P model. The highlighted vapor concentration corresponds to a volume-fraction of 0.6 and, likewise to Figure 2, is shown as a gray iso-surface. In this series of scenes, the transient behavior of the cavitation sheet is shown at three distinct stages: a) the break-up process initiating from the port-side, b) the fragmentation of the central cavity and c) the pinch-off of the main cavitation cloud. During this transition process, the developing cavitation structures appear to provoke the generation of vortices, which grow and accumulate into an unsteady turbulent wake downstream of the cavity. In particular, the results in Figure 3 indicate that the shedding wake is mainly formed by two distinct vortices: i) a weak leakage-vortex induced by the collapsing port-side cavity (Figure 3a) and ii) the primary hairpin vortex which results from the break-up and roll-up of the central cavitation sheet (Figure 3b-3c). The combined pair of vortices create a periodic wake system shedding at two distinct frequencies, resembling a von-Karman vortex street.

Additional information regarding the oscillation dynamics of the simulated cavitation flow is provided in Figure 4. The plotted results correspond to the time history of a) the cavitation volume ($V_{cav.}$), b) the lift-coefficient (C_L) and c) the energy spectrum density (ESD) of the lift force, predicted with the tested cavitation VOF models and turbulent closures. The scatter symbols superimposed on these plots (Figure 4a-4b) correspond to RANS and LES predictions reported at the DelfFoil workshop exercise. Each scatter point represents the time-averaged vapor volume and C_L of the transient flow. These results were calculated using similar cavitation VOF models including the S-S as well as the Zwart models.

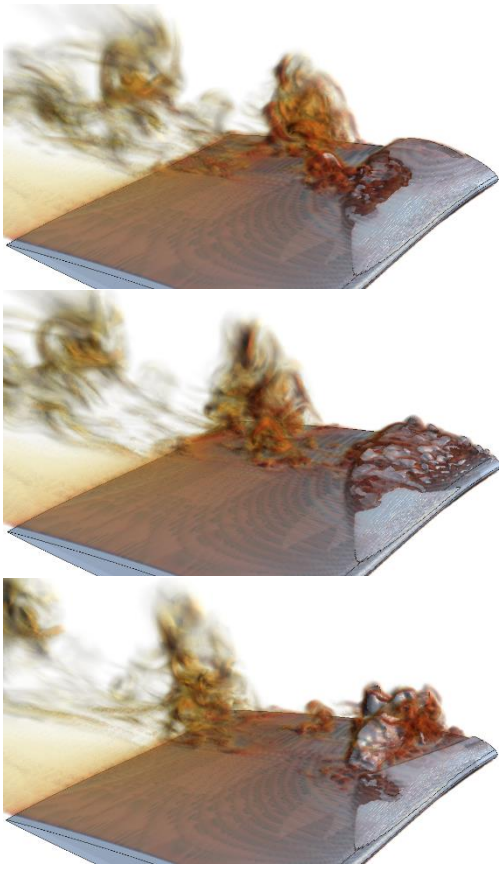

Figure 3: Volume-rendering plots of the vorticity and cavitation volume predicted with the IDDES R-P model

The results published with the asymptotic S-S cavitation model appear comparable to the respective results presented in this study. As shown in Figure 2d, the RANS S-S model underestimated the transient nature of this flow. This is also evident from the predicted weak cavitation oscillations of the sheet cavity (Figure 4a: gray line), following a large initial asymptotic growth stage. Equivalent results using the same two-equation turbulence approach (SST) and the R-P cavitation model indicated a dynamic behavior for the evolving cavitation flow (dark-gray line). In this case, the cavitation sheet performed periodic oscillations and frequently released bubble clouds in the wake (Figure 2c).

Solution differences between the S-S and classical R-P models are also noticeable in the IDDES calculations. As expected, due to the absence of the restoring inertia the cavitation growth/collapse phases are intensified with the asymptotic S-S model (light-gray line), resulting to almost 40% larger cavity sizes compared to the R-P predictions (black line). Depending on the growth/collapse velocity and volume of the shedding cavitation clouds, the induced lift-force exhibits significant negative peaks during the collapse phase. The pressure spikes occur more frequently and with higher amplitudes in the case of the S-S model, as opposed to the relatively damped oscillation predicted with the R-P model (Figure 4b). The mean C_L estimated in the experiment is ≈ 0.5, with an uncertainty limit close to 7%.

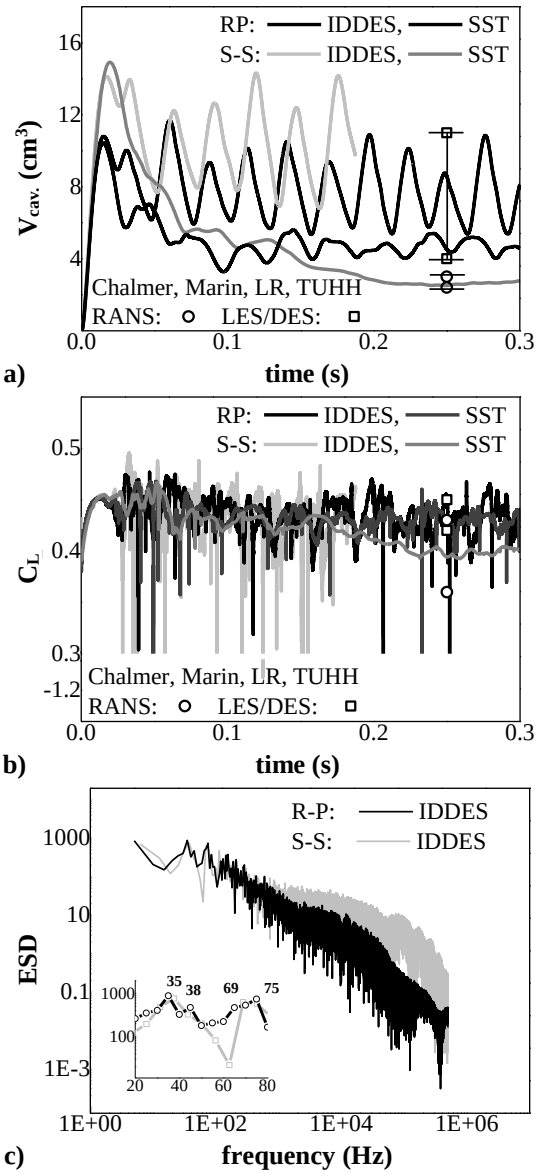

Figure 4: Calculated a) cavitation volume, b) lift-coefficient and c) energy spectrum of the lift force

The turbulent cascade process plotted in Figure 4c suggests that the larger cavitation clouds predicted with the asymptotic S-S model lead to an increase of the energy contained by the inertial eddies, followed by a reduction of the viscous dissipation rates. These conditions seem to accelerate the shedding of the main cavity, which in this case detaches every 26 ms (38 Hz). In the R-P results the mean-flow energy is reorganized more uniformly amongst the spectrum of eddies. This redistribution process regulates the activity of the large-scale eddies and delay the cavitation shedding, which recur every 29 ms (35 Hz). The respective RANS R-P model predicted a lower frequency, close to 32 Hz. The measured shedding frequency in the experiment is in the range of 32 Hz. The second series of higher frequencies predicted by the models corresponds to the secondary leakage cavitation cloud, which sheds prior to the collapse of the main cavity (Figure 3a). This cavitation structure is suppressed with the S-S model, possibly as a result of overestimating the intensity of the primary vortex shedding mechanism.

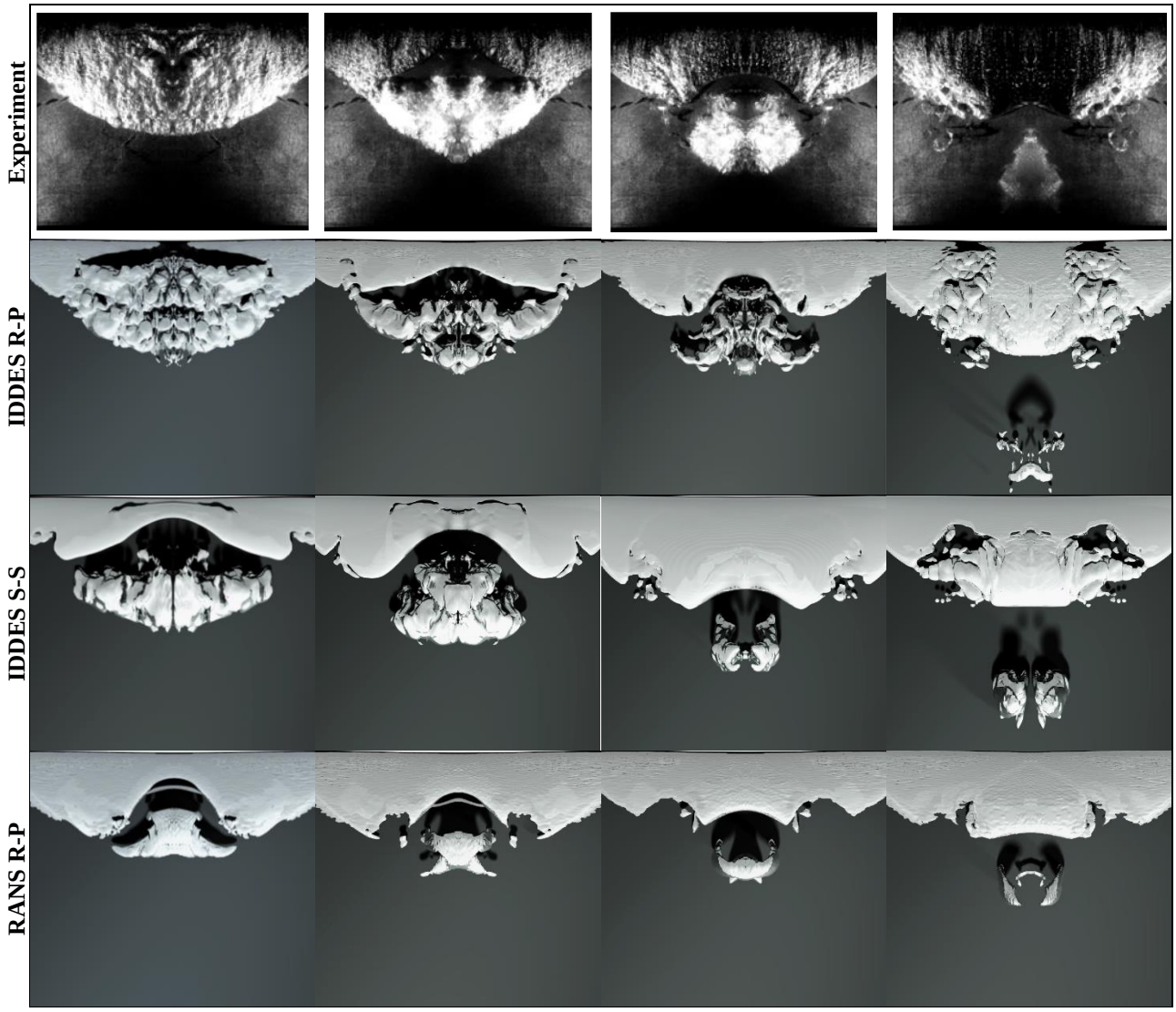

Figure 5: Experimental high-speed flow visualizations (Foeth 2008) and VOF predictions of vortex cavitation shedding

High-speed flow imaging and model predictions of the dynamic cavitation flow are quantitatively compared in Figure 5, for a typical shedding period. The main differences between the S-S and R-P IDDES simulations are the size of the main shedding cloud and the morphology of the predicted cavitation structures. In particular, the R-P model captures a discrete representation of the different cavitation types, resembling small individual clusters of bubbles. A more uniform and continuous cavitation sheet, which transforms into a large shedding cloud, is indicated in the S-S results. The detached cavitation cloud takes the form of a horseshoe vortex and appears to remain more pronounced in time in the S-S model predictions, compared to the experiment where it is shown to rapidly collapse as it departs into the wake.

5 CONCLUDING REMARKS

In this paper the vortex cavitation flow developing on the twist-11 Delft hydrofoil is simulated using the RANS and IDDES solution methods in STAR-CCM+. The two-phase flow is calculated using the Eulerian VOF approach in conjunction with different cavitation models, including the asymptotic S-S as well as the classical R-P models. The obtained results are validated against available experimental measurements as well as compared to corresponding CFD predictions. The results calculated with the IDDES S-S model indicated a higher frequency for the shedding of the main cavity (38 Hz), compared to the experiment (32 Hz). Combined with the SST closure, the S-S model predicted a quasi-steady state cavitation sheet, which performed weak growth/collapse oscillation while remaining attached to the hydrofoil wing. The respective calculations using the classical R-P model captured a dynamic behavior for the evolving cavitation flow, regardless of the utilized turbulence closure. The shedding frequencies calculated with the R-P model are found to be closer to experiment (IDDES: 35Hz, RANS: 32 Hz). In addition, the R-P model predicted the secondary shedding of the leakage vortex, which was underestimated with the asymptotic S-S method. The noted differences in the shedding frequencies predicted by each model are related to the

calculated size and growth/collapse intensity of the cavitation cloud, which are both amplified with the asymptotic S-S approach. Overall, the analysis in this paper converges to the fact that bubble inertial effects have an important role in the dynamics of multiscale cavitation flows with transient character and rapid growth/collapse oscillations.

REFERENCES

Arndt, R. E. A., Arakeri, V. H. & Higuchi, H. (1991). 'Some observations of tip-vortex cavitation'. Journal of Fluid Mechanics, **222**, pp. 269-289.

Arndt, R. E. A. (1995), Chapter XVII Vortex cavitation in Fluid Vortices, Green S. L., Eds. Kluwer Academic Press.

Avellan, F., Dupont, P. & Ryhming, I. (1988). 'Generation mechanism and dynamics of cavitation vortices downstream of a fixed leading edge cavity', Proceedings of the 17th Symposium on Naval Hydrodynamics, Washington, DC.

Batchelor, G. K. (2000). An introduction to Fluid Dynamics, Cambridge University Press.

Bensow, R. E. (2011). 'Simulation of the unsteady cavitation on the Delft Twist22 foil using RANS, DES and LES', 2nd International Symposium on Marine Propulsors, Hamburg, Germany.

Brennen, E. C. (1995). Cavitation and Bubble Dynamics, Oxford University Press.

Foeth, E. J. (2008). 'The structure of three-dimensional sheet cavitation'. PhD Thesis, Delft University of Technology.

Foeth, E. J. & Terwisga, T.v (2006). 'An attached cavity on a three-dimensional hydrofoil'. 6th International Symposium on Cavitation, Wageningen, Netherlands.

Ganesh, H., Mäkiharju, S. A. & Ceccio, S. L. (2016). 'Bubbly shock propagation as a mechanism for sheet-to-cloud transition of partial cavities'. Journal of Fluid Mechanics, **802**, pp. 37-78.

Hoekstra, M., Terwisga, T.v. & Foeth, E. J. (2011). 'smp'11 Workshop – Case 1: DelftFoil'. Second International Symposium on Marine Propulsors, Hamburg, Germany.

Ji, B., Luo, X., Wu, Y., Peng, X. & Duan, Y. (2013). 'Numerical analysis of unsteady cavitating turbulent flow and shedding horse-shoe vortex structure around a twisted hydrofoil'. International Journal of Multiphase Flows, **51**, pp. 33-43.

Johnson, D. A. & King, L. S. (1985). 'A mathematically simple turbulence closure model for attached and separated turbulent boundary layers'. AIAA Journal, **23**, pp. 1684-1692.

Kawanami, Y., Kato, H., Yamaguchi, H., Taminura, M. & Tagaya, Y. (1997). 'Mechanisms and control of cloud cavitation'. Transactions ASME Journal of Fluid Engineering, **119**(4), pp. 788-797.

Knapp, R. T., Daily, J. W. & Hammit, F. G. (1970). Cavitation, McGraw Hill.

Laberteaux, K. R. & Ceccio, S. L. (2001). 'Partial cavity flows. Part 1. Cavities forming on models without spanwise variation'. Journal of Fluid Mechanics, **431**, pp. 1-41.

Lamb, H. (1997). Hydrodynamics, 6th edition, Cambridge University Press.

Leroux, J.-B., C-Delgosha, O. & Astolfi, J. A. (2003). 'A joint experimental and numerical study of mechanisms associated to instability of partial cavitation on two-dimensional hydrofoil'. 5th International Symposium on Cavitation, Osaka, Japan.

Menter, F. R. (1994). 'A Two-equation eddy-viscosity turbulence modeling for engineering applications'. AIAA Journal, **32**(8), pp. 1598-1605.

Rayleigh, L. (1917). 'On the pressure developed in a liquid during the collapse of a spherical cavity'. Philosophical magazine, **34**(200), pp. 94-98.

Reboud, J. L., Stutz, B. & Coutier, O. (1998). 'Two-phase flow structure of cavitation: Experiments and modelling of unsteady effects'. 3rd International Symposium on Cavitation, Grenoble, France.

Plesset, M. S. (1949). 'The dynamics of cavitation bubbles'. Journal of Applied Mechanics, **16**, pp. 277-282.

Sauer, J. (2000). 'Ein neues Modell, basierend auf Front Capturing VOF und Blasendynamik'. PhD Thesis, Universitaet Kalrsruhe.

Schnerr, G. H., Sezal, I. H. & Schmidt, S. J. (2008). 'Numerical investigation of three-dimensional cloud cavitation with special emphasis on the collapse induced shock waves'. Physics of Fluids, **20**.

Singhal, A. K., Athavale, M. M., Li, H. & Jiang Y. (2002). 'Mathematical basis and validation of the full cavitation model'. Journal of Fluids Engineering, **124**(3), pp. 617-624.

Shur, M. L., Spalart, P. R., Strelets, M. K. & Travin, A. K. (2008). 'A hybrid RANS-LES approach with delayed-DES and wall-modelled LES capabilities'. International Journal of Heat and Fluid Flows, **29**, pp. 1638-1649.

Swart. P. J., Gerber, A. G. & Belamri T. (2004). 'A two-phase flow model for predicting cavitation dynamics'. International Conference on Multiphase Flows, **152**, Yokohama, Japan.

Wilcox, D. C. (2008). 'A formulation of the k-ω turbulence model revisited'. AIAA Journal, **46**(11), pp. 2823-283.